Journal of Molecular Liquids 411 (2024) 125766

Contents lists available at ScienceDirect

Journal of Molecular Liquids

journal homepage: www.elsevier.com/locate/molliq

Dissipative particle dynamics simulation and experimental studies of pseudo-gemini surfactants with different hydrophobic chain lengths

Elgun E. Hasanov [a,b], Ravan A. Rahimov [a,b,c,*], Gulnara A. Ahmadova [b], Sevda A. Muradova [d], Atash V. Gurbanov [e,f,g]

[a] Department of Chemical Engineering, Baku Engineering University, Hasan Aliyev str. 120, Baku, Absheron AZ0101, Azerbaijan
[b] Institute of Petrochemical Processes of the Ministry of Science and Education of Azerbaijan, Hojaly ave. 30, AZ 1025 Baku, Azerbaijan
[c] Department of Chemical Engineering, School of Engineering and Applied Science, Khazar University, 41 Mahsati Str., AZ 1096 Baku, Azerbaijan
[d] Department of Medical Microbiology and Immunology, Azerbaijan Medical University, str. S.Vurgun 163, AZ 1078 Baku, Azerbaijan
[e] Centro de Química Estrutural, Institute of Molecular Sciences, Departamento de Engenharia Química, IST-ID Associação do Instituto Superior Técnico para a Investigação e Desenvolvimento, Universidade de Lisboa, 1000-043 Lisboa, Portugal
[f] Excellence Center, Baku State University, Z. Khalilov Str. 23, AZ 1148 Baku, Azerbaijan
[g] Western Caspian University, Istiqlaliyyat Street 31, AZ 1001 Baku, Azerbaijan

ARTICLE INFO

Keywords:
Pseudo-gemini
Piperazine
Carboxylic
Molecular Simulation
DPD

ABSTRACT

In this work new pseudo-gemini type surfactants are constructed via a simple, energy and material efficient way, using piperazine, propylene oxide and seven different fatty acids: capric, lauric, myristic, stearic, oleic and linolenic. The compounds are characterized by ^{1}H NMR, ^{13}C NMR and FTIR studies. Micellization and adsorption properties of the novel pseudo-gemini surfactants are investigated via surface tension and conductivity measurements. Antimicrobial properties are evaluated using the simple disk diffusion test method. Dissipative Particle Dynamics (DPD) simulations are performed to model aggregation behavior of the new pseudo-gemini surfactants. Experimental studies revealed that Critical Micelle Concentration (CMC) of the obtained pseudo-gemini surfactants are lower than 1 mmol/L. Theoretically calculated CMC values are slightly higher than experimental CMC values. However, overall, very good agreement between theoretical and experimental CMC values is observed. Radial Distribution Function (RDF) and radius of gyration (R_g) plots are analyzed to gain further insight into aggregation of the surfactant molecules in aqueous environment. The DPD model of the pseudo-gemini amphiphiles successfully predicts the most important traits of the aggregation process.

1. Introduction

Gemini structured surfactants have been known to researchers for over two decades and have been praised for their superior performance in comparison to conventional surfactants [1]. The construction of gemini surfactants involves bringing two hydrophobic and two hydrophilic molecular fragments together using covalent bonding [2]. While gemini or dimeric surfactants found applications in varying fields of science and technology such as medicine, nanoscience, optics, electronics, enhanced oil recovery [3,4], chemical catalysis [5–8], trimeric [9–11], even tetrameric [12–14] surfactants with eye-catching application properties have been synthesized. However, common synthesis methods of gemini surfactants involve application of heating and refluxing techniques for several days until the reaction is complete [2–4,15]. This introduces limitations on development of novel surface-active compounds and brings about sustainability issues from material and energy usage point of view.

Gemini-like amphiphilic systems can be designed utilizing non-covalent interactions between a single-chain surface-active molecule and a di-cationic counterion. This method of constructing gemini-like or pseudo-gemini structures is more energy-efficient and material-efficient in comparison to conventional covalent synthesis. Over the years numerous pseudo-gemini surfactant systems have been designed and their valuable application properties have been investigated. Jia et al. [16] constructed such system utilizing noncovalent interaction between anionic surface-active compound sodium dodecyl benzene sulfonate (SDBS) and 4,4′-oxydianiline (ODA). They investigated the surface activity and emulsification behavior of the pseudo-gemini surfactant

* Corresponding author at: Department of Chemical Engineering, Baku Engineering University, Hasan Aliyev str. 120, Baku, Absheron AZ0101, Azerbaijan.
E-mail address: rarahimov@beu.edu.az (R.A. Rahimov).

https://doi.org/10.1016/j.molliq.2024.125766
Received 21 June 2024; Received in revised form 1 August 2024; Accepted 13 August 2024
Available online 14 August 2024

system by modifying the pH and concentration of aqueous solutions. Zhang and coworkers [17] obtained pseudo-gemini amphiphiles from erucamido-propyl dimethylamine and 5-sulfoisophthalic acid. The pseudo-gemini amphiphiles exhibited good viscoelastic behavior in aqueous solution. The surfactant solutions had dual function of fracturing fluid and oil flooding with high oil washing efficiency. Ye et al. [18] prepared a pH-responsive surfactant N-decyl-maleimidepimaric acid N, N-dimethylenediamide (C_{10}MPAN) from rosin via a three-step process. Then pseudo-gemini amphiphilic structures were constructed by mixing C_{10}MPAN with maleic acid in a 2:1 M ratio. The formation of viscoelastic solutions and hydrogels was triggered by reducing the pH of aqueous solution of C_{10}MPAN-maleic acid type pseudo-gemini surfactants. Wei and others [19] synthesized pseudo-tetrameric surfactants by mixing different cyclic amines (1,4,7,10-tetraazacyclododecane; 1,4,7,10-tetraazacyclotridecane; 1,4,8,11-tetraazacyclotetradecane and 1,4,8,12-tetraazacyclopentadecan) and stearic acid in 1:4 mol ratio. They investigated CO_2-switchable behavior of the aqueous pseudo-tetrameric surfactant solutions. Injection of CO_2 to the surfactant solutions resulted in a decrease of solution viscosity by a few orders of magnitude. Upon removal of CO_2 from solution viscosity increased to its initial values. The authors noted the potential applicability of the CO_2-switchable tetrameric surfactants for enhanced oil recovery. Another pseudo-tetrameric surfactant was synthesized by Chen et al. [20] from a monomer containing four quaternized nitrogen atoms and azo-benzene group (Tetra-N(AZO)-Br), and sodium oleate. Tetra-N(AZO)-Br and sodium oleate were mixed in 1:4 M ratio to obtain the pseudo-tetrameric surface-active compounds. Aqueous solutions of the pseudo-tetrameric surfactant displayed viscoelastic behavior. Due to presence of the azo group the pseudo-tetrameric surfactant was UV-sensitive which was evidenced by obvious color change of the solutions upon UV light exposure. However, irradiation with UV light did not alter the viscoelastic properties of the surfactant solutions.

In the current study, we report the synthesis of pseudo-gemini amphiphilic structures designed using commercially available, low-cost materials, utilizing a heating-free and reflux-free reaction procedure. In addition, DPD simulation of the surfactant-water systems comprised of the aqueous solutions of the obtained pseudo-gemini surfactants is performed. The main goal of the study is to demonstrate the synthesis and physicochemical properties of novel surface-active materials based on piperazine, propylene oxide and fatty acids of varying chain length and structure. In addition, molecular simulation study of the surfactants was performed to explore the effectiveness of DPD methodology in predicting properties of pseudo-gemini type amphiphiles. Fatty acids are biologically compatible compounds that are prepared from renewable sources [21]. Piperazine is the structural backbone of many biologically active compounds and is manufactured in large quantities through commercial synthesis procedures [22]. Propylene oxide is an effective alkylating agent and is also produced in significant quantities via various industrial processes [23]. This work can act as an inspiration for exploration of methods to construct surface-active materials in a “green” and economical way.

2. Experimental section

2.1. Reagents

Piperazine (99 %), capric acid (98 %), lauric acid (98 %), myristic acid (98 %), palmitic acid (98 %), stearic acid (97 %) and linolenic acid (99 %) were products of Sigma-Aldrich. Oleic acid (99 %) was purchased from Alfa Aesar. Propylene oxide (99 %) was the product of Azerikimya. All chemicals were used as received.

2.2. Synthesis

Pseudo-gemini surfactants were synthesized via the reaction pathway described in Scheme 1. The first step is the synthesis of 1,4-di-(propane-2-olyl)-piperazine and the second step is the neutralization of the amine derivative with fatty acids. 1,4-di-(propane-2-olyl)-piperazine was synthesized through the epoxide ring opening reaction propylene oxide with piperazine in 2:1 M ratio. The reaction was performed at room temperature without solvent, under pH-neutral conditions (Step 1 in Scheme 1). Finely crushed crystals of piperazine were added to the reaction flask with excess amount of propylene oxide to achieve complete conversion of piperazine. Excess amount of propylene oxide was later removed with vacuum evaporation. The ring opening of epoxides in presence of amines at neutral and basic environment was described by Sundaram and Sharma [24].

Pseudo-gemini surfactants were prepared by mixing 1,4-di-(propane-2-olyl)-piperazine with six different fatty acids (capric, lauric, myristic, palmitic, stearic, oleic, linolenic) in 1:2 M ratio (Step 2 in Scheme 1). Fine crystals of 1,4-di-(propane-2-olyl)-piperazine were added to a flask with a fatty acid measured in 1:2 M amount. The reagents were dissolved in pure acetone and the solution was kept still for a few hours before evaporating acetone under vacuum. The products were used without further purification.

2.3. Characterization of products

FTIR (Bruker LUMOS FT-IR, neat samples), ^{1}H NMR, and ^{13}C NMR (Bruker BioSpin, 400.13 MHz and 100.62 MHz, $CDCl_3$) analysis were performed for characterization of the synthesized compounds. IR, ^{1}H NMR and ^{13}C NMR spectra of the compounds are included in the Supporting Information.

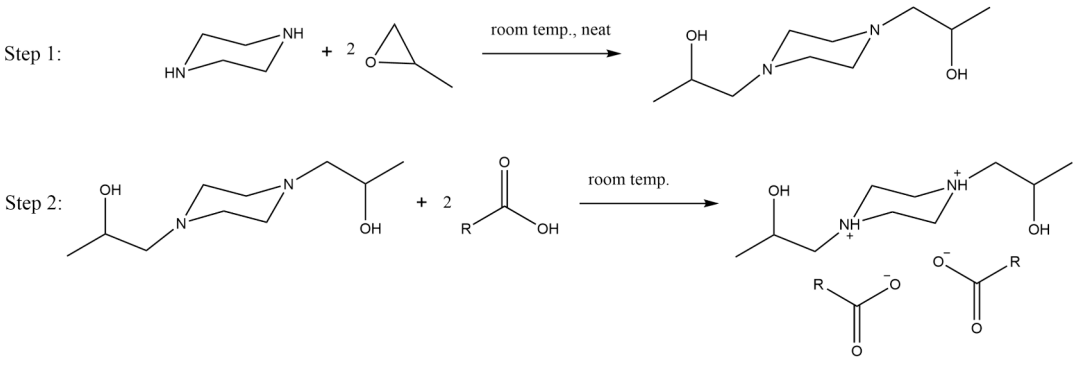

R = C_9H_{19}, $C_{11}H_{23}$, $C_{13}H_{27}$, $C_{15}H_{31}$, $C_{17}H_{35}$, CH_3-$(CH_2)_7$-CH=CH-$(CH_2)_7$, CH_3-CH_2-CH=CH-CH_2-CH=CH-CH_2-CH=CH-$(CH_2)_7$

Scheme 1. Synthesis of pseudo-gemini surfactants from piperazine and fatty acids.

2.4. Surface tension measurement

Surface tension measurements were performed with a Attension® Sigma 702 tensiometer (Biolin Scientific, Finland). Surface tension of the distilled water used for preparing solutions was measured to be 71.5 mN/m at 25 °C. The measurements were repeated three times to ensure reproducibility of data, and the average value was recorded (accurate to 0.01 mN/m).

2.5. Electrolytic conductivity measurement

Electrolytic conductivity measurements were performed with a CO 3000L benchtop conductivity meter (VWR® pHenomenal®, Germany) equipped with a pHenomenal® CO 11 conductivity sensor using a graphite electrode. The cell constant of the conductivity sensor was set to 0.84 cm^{-1}. Conductivity values were recorded at a reference temperature of 25 °C and were accurate to ±1 %. Specific conductivity of double distilled water was in the 1.2–1.5 μS/cm range. The measurements were performed three times to ensure reproducibility of data, and the average value was recorded. Krafft temperatures were also determined with conductometry method [25].

2.6. Dynamic Light Scattering (DLS)

Aggregate size distribution of the synthesized surfactants was investigated using DLS method with a Horiba LB-550 particle size analyzer (Horiba Scientific, Japan). The samples were scanned at 25 °C with a 650 nm laser diode generating a 5mW light beam. Particles from 1 nm to 6000 nm hydrodynamic radius were scanned. The size distribution data was generated using CONTIN algorithm. The average of three distinct measurements was recorded.

2.7. Antimicrobial properties

Antimicrobial properties of the obtained surfactants were tested using modified Kirby-Bauer disk diffusion method. The tests were conducted with meat-peptone agar inoculated with various gram-negative (*Escherichia coli*, *Pseudomonas aeruginosa*, *Klebsiella pneumoniae*) and gram-positive (*Staphylococcus aureus* (MRSA), *Bacillus anthracis*) bacteria, in addition Sabouraud agar inoculated with fungal microorganism *Candida albicans*. The concentration of the broth suspensions was kept at 500 mln cells per mL. The agar plates were incubated at 37 °C for 24 h prior to the tests. 6 mm diameter filter paper disks loaded with the surfactants were placed onto the agar plates to determine the diameter of inhibition zone.

3. Dissipative particle Dynamics (DPD) study

3.1. DPD method

DPD is an effective method for theoretical study of self-assembling materials such as surfactant systems. The method was first developed by Hoogerbrugge and Koelman [26] and later was revisited and revised by Español [27]. DPD is a coarse-grained molecular simulation method that offers good trade-off between computational power and simulation time scale. In coarse-grained methods molecular fragments that consist of more than a single heavy atom (atoms other than hydrogen) are modelled as single particles called “beads”. The DPD algorithm solves Newton’s classical laws of motion equations to determine the final position and momenta of the bead particles, and as a result displays the final configuration of the system in mesoscopic scale. DPD methodology was applied to explore theoretical properties of surfactant-water system formed in aqueous solutions of the obtained pseudo-gemini surfactants.

3.2. Atom to bead mapping

Surfactant molecules were divided into fragments of 3 or 4 heavy atoms whereas water molecules were combined into a group of 3 (N_m = 3) in-line with a work by Groot and Rabone [28], to form bead particles. Bead mapping scheme for the DPD simulations is presented in Fig. 1. The best practice for bead mapping in DPD is to choose bead volumes to be approximately the same. The volume of a single water molecule is generally taken to be equal to 30 $Å^3$ [28]. Thus, the effective volume of a water (W) bead would be equal to $3 \times 30 = 90$ $Å^3$. The molecular volume of each one of the bead particles was calculated using Gaussian 09 software and are listed in Table 1. The volume of each bead was set to an adjusted volume of 90 $Å^3$. Bead density was chosen as $\rho = 3$ as recommended by Groot and Warren [29]. Effective bead diameter is taken to be equal to bead interaction cutoff radius (r_C) and is calculated using the Eq. (1) deduced from Groot and Rabone [28]:

$$r_c = \sqrt[3]{\rho V_{bead}} \tag{1}$$

where ρ is dimensionless bead density and V_{bead} is bead volume in $Å^3$. Therefore, the effective bead diameter is $r_C = \sqrt[3]{(3 \times 90\ Å^3)} = 6.46$ Å.

3.3. DPD forces

DPD simulation calculates the forces acting on the bead particles from both non-bonded and bonded interactions:

$$F_i = \sum_{i \neq j \neq k} F_{ij}^C + F_{ij}^D + F_{ij}^R + F_{ij}^E + F_{ij}^S + F_{ijk}^A \tag{2}$$

The first four terms in Eq. (2) above are related to non-bonded interactions between a pair of particles. F_{ij} signifies the force acting on bead i by bead j. F_{ij}^C is the conservative force, F_{ij}^D is the dissipative force, F_{ij}^R is the random force, and F_{ij}^E is the electrostatic force. The last two terms are bonded interactions: F_{ij}^S is called the spring force and F_{ij}^A is related to angular stiffness of the bonds.

The conservative force is a repulsive force. It takes into account the chemical and physical characteristics of all involved particles. The following soft harmonic form of conservative force was applied:

$$F_{ij}^C = \begin{cases} a_{ij}\left(1 - \frac{r_{ij}}{r_C}\right) e_{ij} & r_{ij} < r_C \\ 0 & r_{ij} \geq r_C \end{cases} \tag{3}$$

where a_{ij} is an interaction parameter between beads i and j, r_C is the cut-off radius. r_{ij} is the distance between beads i and j. e_{ij} is the unit vector where $e_{ij} = r_{ij}/|r_{ij}|$.

The dissipative force is proportional to the velocity of two approaching particles and accounts for the friction experienced by the beads. The dissipative force is expressed by:

$$F_{ij}^D = -\gamma_{ij}\omega^D(r_{ij})(v_{ij} \bullet e_{ij})e_{ij} \tag{4}$$

γ_{ij} is the friction coefficient between two beads and $\gamma_{ij} = \gamma_{ji} > 0$. $v_{ij} = v_i$-v_j is the velocity difference between two particles. ω^D is a distance dependent weight function of form:

$$\omega^D = \begin{cases} \left(1 - \frac{r_{ij}}{r_C}\right)^2 & r_{ij} < r_C \\ 0 & r_{ij} \geq r_C \end{cases} \tag{5}$$

The random force expresses the effect of random motion of the particles in the system and takes the following form:

$$F_{ij}^R = \sigma_{ij}\omega^R(r_{ij})\xi_{ij}\frac{1}{\sqrt{\Delta t}}e_{ij} \tag{6}$$

σ_{ij} is the noise amplitude, where $\sigma_{ij} = \sigma_{ji} > 0$. ω^R is a distance dependent

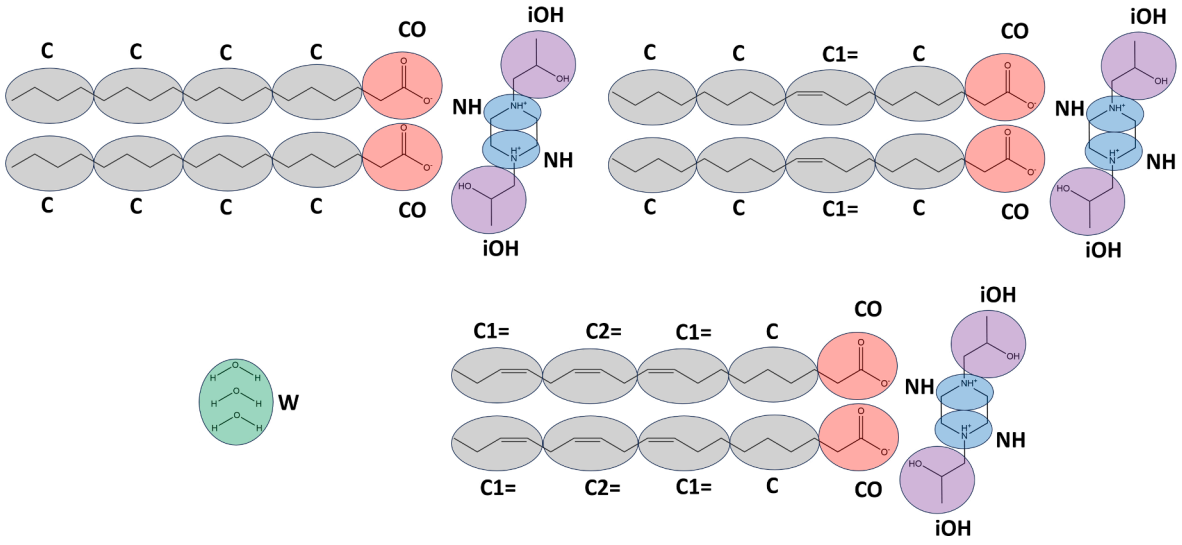

Fig. 1. Bead mapping scheme.

Table 1
Bead dimensions.

Bead type	Equivalent compound	Molecular volume, Å^3	Adjusted bead volume, Å^3	Bead diameter, Å
C	C_4H_{10}	100.07	90	6.46
C1=	$CH_2 = CHC_2H_5$	108.55	90	6.46
C2=	$CH_3CH = CHCH_3$	104.53	90	6.46
CO	CH_3COOH	72.49	90	6.46
iOH	CH_3CHCH_3OH	96.27	90	6.46
NH	CH_3NHCH_3	84.41	90	6.46
W	$3{\cdot}H_2O$	84.81	90	6.46

weight function, $\xi_{ij} = \xi_{ji} > 0$ is a randomly fluctuating Gaussian variable with a zero mean and unit variance, Δt is the time step used when solving the terms in the equation for force on an individual bead.

The noise amplitude σ_{ij} is related to γ_{ij} in the following way:

$$\sigma_{ij}^2 = 2\gamma_{ij}k_BT \tag{7}$$

where k_B is the Boltzmann constant ($k_B = 1.380649 \times 10^{-23}$ J·K^{-1}) and T is the absolute temperature in K.

The weight functions of the dissipative and random force are related to each other:

$$\omega^D = (\omega^R)^2 \tag{8}$$

The dissipative and random forces together form a DPD thermostat, maintaining the temperature of the simulated system.

The electrostatic interaction between charged beads was represented by the electrostatic force of Coulombic form:

$$F_{ij}^E = k_e\frac{q_iq_j}{\varepsilon_r r_{ij}^2} \tag{9}$$

where k_e is the Coulomb's constant ($k_e = 8.99 \times 10^9 N \cdot m^2 \cdot C^{-2}$), q_i and q_j are the charges of the beads i and j, ε_r is the relative permittivity of the medium.

In our DPD simulation the bonds between beads are modelled as springs with harmonic potential. The functional form of the spring force and potential are expressed with the following equations:

$$F_{ij}^S = -\frac{\delta U^S}{\delta r_{ij}} \tag{10}$$

$$U^S = \sum_j \frac{1}{2}C^b(r_{ij} - r_0)^2 \tag{11}$$

where C^b is the spring constant in DPD units, r_0 (in DPD units) is unstretched bond length between particles i and j.

Angle bend between two adjacent bonds is represented by the angular force F_{ijk}^A of cosine harmonic form:

$$F_{ij}^A = -\frac{\delta U^A}{\delta r_{ij}} \tag{12}$$

$$U^A = \sum_j \frac{1}{2}C^a(\cos\theta_{ijk} - \cos\theta_0)^2 \tag{13}$$

where C^a is angle constant in DPD units, θ_{ijk} is bond angle, θ_0 is the equilibrium bond angle.

3.4. DPD parameters

3.4.1. Non-bonded interaction parameters

The repulsion parameter a_{ij} in Eq. (3) is related to Flory-Huggins chi-parameters (χ_{ij}) by Groot and Rabone [28] (for $\rho = 3$):

$$a_{ij} = a_{ii} + \frac{\chi_{ij}}{0.231} \tag{14}$$

The Flory-Huggins chi-parameters (χ_{ij}) for all bead pairs have been estimated using the Blends module in Materials Studio 2023 software and included in the Supporting Information (see Table S1).

In the Eq. (14) above a_{ii} is the interaction parameter between identical beads and calculated using the following equation [29]:

$$a_{ii} = \frac{(16N_m - 1)k_BT}{0.2\rho} \tag{15}$$

The values of a_{ij} and a_{ii} have been calculated for all bead pairs and included in Table 2.

The friction coefficient γ_{ij} was taken to be equal to 4.5 (in DPD units) based on the recommended value in literature [29,31–35].

Time step Δt was set to $\Delta t = 0.01$ [30,34], $\Delta t = 0.04$ [29,35], $\Delta t = 0.05$ [33], and $\Delta t = 0.06$ [28,32] in different works by others. Selection of smaller time steps can improve accuracy of the simulation results in the expense of longer runtimes and higher computational cost. However, the improvement of simulation results with smaller time steps can be marginal and might not always justify the additional computational

Table 2
Bead pair interaction parameter, a_{ij} (in DPD units).

Bead type	C	C1=	C2=	CO	iOH	NH	W
C	78.33						
C1=	78.38	78.33					
C2=	78.44	78.32	78.33				
CO	133.5	131.0	129.9	78.33			
iOH	89.11	87.83	87.93	91.75	78.33		
NH	82.23	81.51	81.48	79.82	73.02	78.33	
W	118.8	114.5	115.0	80.53	74.88	73.87	78.33

effort [35]. We chose a time step of $\Delta t = 0.05$ (in DPD units) to get good accuracy with optimum computational efficiency.

NH and CO beads were assigned electrostatic charges of +1 and −1 respectively, while all other beads were assigned 0 charge. The relative permittivity ε_r was set to 78.2 (value for water at 25 °C) to simulate the aqueous environment.

3.4.2. Bonded interaction parameters

The spring constant value of $C^b = 150$ (DPD units) was adopted for all bonds [30,34,36]. The unstretched bond length r_0 for all bead pairs was calculated based on the number of heavy atoms in each bead (n_i and n_j) as following [30]:

$$r_0 = 0.1(n_i + n_j) - 0.01 \quad (16)$$

For example, unstretched bond length of [NH]–[iOH] ([CH_3NHCH_3]–[CH_3CHCH_3OH]) bond would be $r_0 = 0.1 \times (3 + 4)$-0.01 = 0.69 in DPD units.

The value of angle constant for all bond angles were set to $C^a = 5$. Equilibrium angle of $\theta_0 = 180°$ was selected for all bond angles [30,34,36] in case of pseudo-gemini surfactants constructed from saturated fatty acids (see Table S2). For $C_{18:1}$-$PiPO_2$-$C_{18:1}$ and $C_{18:3}$-$PiPO_2$-$C_{18:3}$, the geometries of oleic acid and linolenic acid molecules were optimized in Gaussian 09 to approximate the equilibrium bond angles to use in the DPD coarse grained model (see Figure S9).

3.4.3. Simulation details

Simulation box of 30 × 30 × 30 ($L_x \times L_y \times L_z$) was set up and 94,000 beads were randomly added to the simulation box. Various surfactant concentrations (2 mM, 5 mM, 10 mM, 20 mM) were simulated. Simulations were run for 100,000 steps to achieve thermodynamic equilibrium. The temperature was kept constant at 298 K and the volume of the simulation box was not changed.

4. Results and discussion

4.1. Surface activity and micellization

The variation of surface tension with concentration of the pseudo-gemini surfactants is presented in Fig. 2. Each one of the surfactants exhibits high surface activity. Short chain pseudo-gemini surfactants achieved lower value of minimum surface tension in comparison to their longer chain homologues. Overall, recorded minimum surface tension values are in the range of 22 mN/m and 35 mN/m.

The CMC is the minimum bulk concentration of the surfactant at a given temperature required for formation of self-assembled clusters of molecules, aka micelles, in solution environment. CMC values determined from the conductometric measurements are listed in Table 3. Pseudo-gemini surfactants constructed from piperazine derivative and fatty acids have CMC values in 0.171–0.779 mmol/L range. Theoretically, CMC values are expected to decrease with increasing hydrophobic chain length. However, this trend is disrupted for the surface-active compounds reported in this work. This disruption can be explained by relatively low solubility of pseudo-gemini surfactants with C_{14}, C_{16} and C_{18} tails as expressed by high Krafft points (see Table 3).

Conductometric CMC values are marked with hollow circles on the

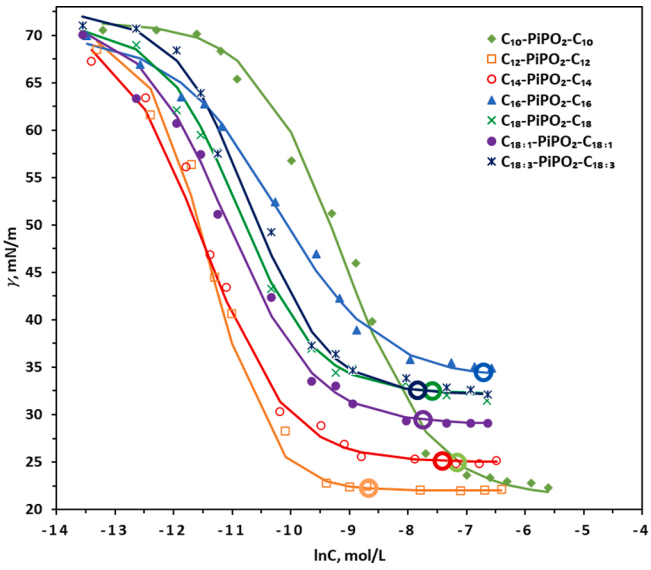

Fig. 2. Gibbs adsorption isotherms of the obtained pseudo-gemini surfactants.

Gibbs adsorption isotherm plots (see Fig. 2) and are at the stabilized region of the adsorption isotherms. This is indicative of a good agreement between tensiometric and conductometric determination of CMC values.

Maximum surface excess concentration (Γ_{max}) is related to the number of surfactant molecules adsorbed at the surface or interface and is one of the crucial parameters used to evaluate adsorption behavior of a surface-active compound. It was calculated from the surface tension data using the Eq. (17) below [37]:

$$\Gamma_{max} = -\frac{1}{nRT}\lim_{C \to CMC}\frac{d\gamma}{d\ln C} \quad (17)$$

where R is the universal gas constant (8.314 J mol^{-1} K^{-1}), C is the concentration of surfactant, T is the absolute temperature in K, and γ is the surface tension. The effective number of molecular species at the interface was chosen as n = 3 because of rigid spacer and bulky divalent cation, in accordance with the conclusions of neutron reflectivity study by Li et al. [38].

The minimum surface area per molecule in square angstroms ($Å^2$) was calculated for each surfactant with the Eq. (18) [37]:

$$A_{min} = \frac{10^{16}}{N_A \Gamma_{max}} \quad (18)$$

The minimum surface area per molecule A_{min} decreases as more surfactant molecules are becoming adsorbed at the interface. The values of maximum surface excess concentration Γ_{max} and minimum surface area per molecule A_{min} have been listed in Table 3.

Pseudo-gemini surfactants C_{14}-$PiPO_2$-C_{14}, C_{16}-$PiPO_2$-C_{16} and C_{18}-$PiPO_2$-C_{18} have high Krafft points and relatively high values of A_{min} in comparison to C_{10}-$PiPO_2$-C_{10} and C_{12}-$PiPO_2$-C_{12}. In addition, achieved minimum surface tension for the saturated chain pseudo-gemini amphiphiles mentioned above increases with increasing alkyl chain length (see Fig. 2). It can be inferred that relatively poor solubility of saturated middle and high chain amphiphiles resulted in inferior adsorption at the water–air interface.

Each one of the pseudo-gemini surfactants C_{18}-$PiPO_2$-C_{18}, $C_{18:1}$-$PiPO_2$-$C_{18:1}$ and $C_{18:3}$-$PiPO_2$-$C_{18:3}$ has 18 carbon atoms in their hydrophobic fragments. Among the three surfactants the ones with unsaturated oleate ($C_{18:1}$-$PiPO_2$-$C_{18:1}$) and linolenate ($C_{18:3}$-$PiPO_2$-$C_{18:3}$) tail groups have higher area per molecule in comparison to C_{18}-$PiPO_2$-C_{18}, which has saturated stearate tails. This can be explained by the fact that the double bonds in the hydrocarbon chains of $C_{18:1}$-$PiPO_2$-$C_{18:1}$ and

Table 3
Physicochemical parameters of gemini-like surfactants based on 1,4-di-(propane-2-olyl)-piperazine and fatty acids at 25 °C[a].

Surfactant	Krafft point [°C]	CMC [mmol/L]	$\Gamma_{max} \times 10^{10}$ [mol/cm^2]	A_{min} [Å^2]	β	ΔG^0_{mic} [kJ/mol]	ΔG^0_{ads} [kJ/mol]
C_{10}-$PiPO_2$-C_{10}	<0 °C	0.779	1.475	112.61	0.253	−21.70	−24.85
C_{12}-$PiPO_2$-C_{12}	<0 °C	0.171	1.392	119.33	0.654	−37.14	−40.68
C_{14}-$PiPO_2$-C_{14}	13 °C	0.600	1.240	133.92	0.447	−27.68	−31.42
C_{16}-$PiPO_2$-C_{16}	18 °C	0.677	1.007	164.85	0.271	–22.47	−26.09
C_{18}-$PiPO_2$-C_{18}	11 °C	0.528	1.321	125.74	0.260	–22.64	−25.60
$C_{18:1}$-$PiPO_2$-$C_{18:1}$	<0 °C	0.612	1.082	153.48	0.214	−21.05	−24.95
$C_{18:3}$-$PiPO_2$-$C_{18:3}$	<0 °C	0.586	1.124	147.76	0.354	−25.11	−28.59

[a] The standard uncertainties (u) are u(T) = 0.1 °C and u(p) = 10 kPa. The combined expanded uncertainties U_c are $U_c(\gamma) = 0.1$ mN/m, U_c(CMC) = 4×10^{-3} mmol/L, $U_c(\pi) = 0.1$ mN/m, $U_c(\Gamma_{max}) = 0.05$ mol/cm^2, $U_c(A_{min}) = 0.8$ Å^2, $U_c(\beta) = 0.03$, and $U_c(\Delta G) = 0.05$ kJ/mol (0.68 level of confidence).

$C_{18:3}$-$PiPO_2$-$C_{18:3}$ result in bent geometry of the tail groups and hinders efficient packing of the molecules at the interface.

The degree of counterion binding to the micelles (β) was calculated using the Eq. (19) below [37]:

$$\beta = 1 - \alpha = 1 - \frac{S_1}{S_2} \tag{19}$$

Where S_2 and S_1 represent the slope of conductivity (κ) vs. concentration plots below and above the CMC point, respectively (see Figs. S1-S7). The counterion binding degree expresses the fraction of an ionic surfactant's counterions that are in association with the micelles. For example, if the concentration of the surfactant molecules that are included in the micelles is C_{Mic}, then the concentration of counterions bound to the micelles would be expressed as (1-α)•C_{Mic}. Then the bulk concentration of the total surfactant molecules dissolved would be $C_T = C_{Mic} + C_{Mon}$, where C_{Mon} is the concentration of surfactants in their monomeric form, i.e., not participating in micelle formation [39].

There is an inverse relationship between CMC values and counterion binding degrees of the pseudo-gemini surfactants reported in this work (see Fig. S8). Sugihara and Hisatomi [40] also reported the inverse relationship between CMC and β values of various types of monomeric and gemini surfactants in aqueous environment.

4.2. Thermodynamics of micellization and adsorption

The standard Gibbs free energy of micellization indicates the spontaneity of micellization. The Eq. (20) below suggested by Zana [41] was used to calculate the Gibbs free energy of micellization:

$$\Delta G^0_{mic} = RT(0.5 + \beta)\ln X_{CMC} - \left(\frac{RT}{2}\right)\ln 2 \tag{20}$$

where X_{CMC} indicates the mole fraction of surfactant at CMC.

The standard Gibbs free energy of adsorption was calculated with the Eq. (21) below [37]:

$$\Delta G^0_{ad} = \Delta G^0_{mic} - 0.6023\pi_{CMC}A_{min} \tag{21}$$

where π_{CMC} is the surface tension reduction at CMC. The calculated values of ΔG^0_{mic} and ΔG^0_{ads} are shown in Table 3. Thermodynamic properties of the pseudo-gemini surfactants with fatty acid fragments seem to be influenced by various factors including solubility, alkyl chain length and alkyl chain geometry of their hydrophobic moieties. The optimum balance of these properties resulted in lower values of ΔG^0_{mic} and ΔG^0_{ads}.

4.3. Dynamic Light Scattering (DLS)

Aggregate size distributions of the investigated pseudo-gemini surfactants have been determined at 1 × CMC and 2 × CMC (see Fig. 3). Short alkyl chain surfactants C_{10}-$PiPO_2$-C_{10}, C_{12}-$PiPO_2$-C_{12} and C_{14}-$PiPO_2$-C_{14} have mean aggregate size of 3.2–3.6 nm at 1 × CMC solution concentration. Mean aggregate size of $C_{18:3}$-$PiPO_2$-$C_{18:3}$ is 4.4 nm at 1 × CMC, despite its long alkyl chain. Mean aggregate sizes of C_{16}-$PiPO_2$-C_{16}, C_{18}-$PiPO_2$-C_{18} and $C_{18:1}$-$PiPO_2$-$C_{18:1}$ in 1 × CMC concentration solutions are 2040 nm, 1338 nm, and 151 nm, respectively. Aggregate size distribution curves of C_{10}-$PiPO_2$-C_{10}, C_{12}-$PiPO_2$-C_{12} and $C_{18:3}$-$PiPO_2$-$C_{18:3}$ are essentially unaffected by concentration shifting to 2 × CMC. Aggregate sizes of C_{18}-$PiPO_2$-C_{18} and $C_{18:1}$-$PiPO_2$-$C_{18:1}$ do not show a major shift upon raising the concentration to 2 × CMC, except for their bimodal distribution curves at 2 × CMC. Overall, only C_{14}-$PiPO_2$-C_{14} exhibits a major jump in aggregate sizes upon shifting from 1 × CMC to 2 × CMC. Size distribution peaks shown in Fig. 3 belonging to aggregates smaller than about 10 nm usually indicate presence of simple spherical

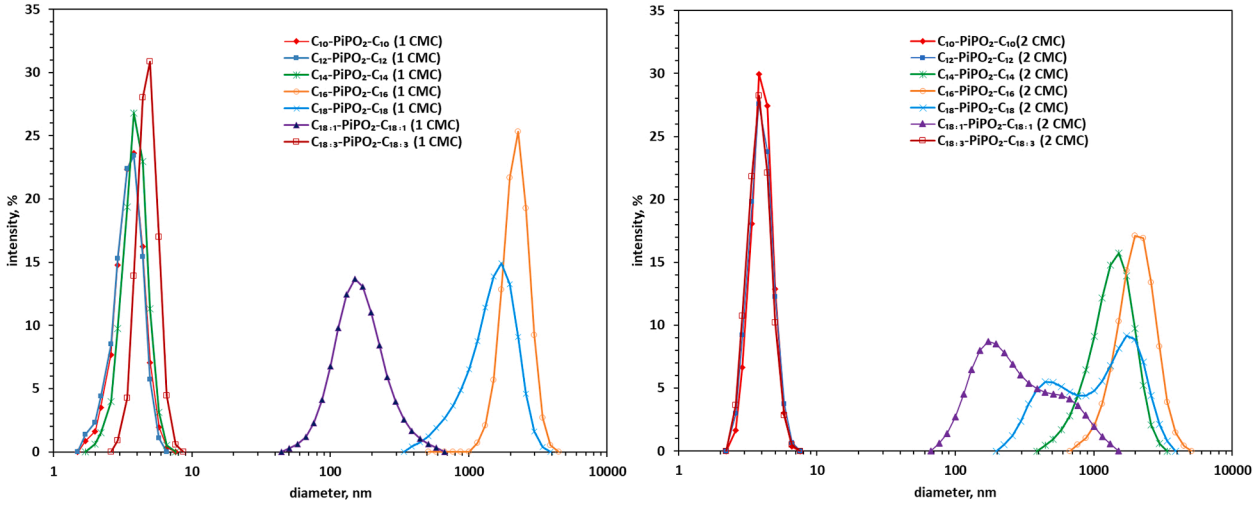

Fig. 3. DLS measured aggregate size distribution of pseudo-gemini surfactants.

micelles. Aggregate size distribution curves of C_{16}-$PiPO_2$-C_{16}, C_{18}-$PiPO_2$-C_{18} and $C_{18:1}$-$PiPO_2$-$C_{18:1}$ signal more complex multi-micelle aggregate structures [42]. Overall, pseudo-gemini surfactants with shorter alkyl chain form smaller aggreates as expected. Surfactants with unsaturated bond in the alkyl chain also tend to have smaller mean aggregate sizes due to geometric constraints introduced by the double bonds. Mean aggregate sizes of C_{16}-$PiPO_2$-C_{16} is greater than that of C_{18}-$PiPO_2$-C_{18} despite having shorter hydrocarbon chain. This anomaly can be explained by the higher CMC of C_{16}-$PiPO_2$-C_{16} in comparison to C_{18}-$PiPO_2$-C_{18}.

4.4. Antimicrobial properties

The results of antimicrobial susceptibility tests performed on pseudo-gemini type surfactants have been presented in Table 4. The effect of antimicrobial agent is deemed as strong if the inhibition zone diameter is >25 mm, moderate if in 15–25 mm range, and weak if <15 mm. The overall antimicrobial performance of the pseudo-gemini amphiphiles constructed from piperazine derivative and fatty acids is not strong. Short alkyl chain surfactant C_{10}-$PiPO_2$-C_{10} and unsaturated chain surfactants $C_{18:1}$-$PiPO_2$-$C_{18:1}$ and $C_{18:3}$-$PiPO_2$-$C_{18:3}$ displayed better overall antimicrobial performance compared to other surfactants with saturated alkyl chain. Gram-negative *Pseudomonas aeruginosa* displayed the highest resistance to pseudo-gemini surfactants. Overall, the pseudo-gemini surfactants had better antimicrobial effect on gram-positive bacteria and fungal microorganism *Candida albicans*.

Antimicrobial properties of standard antimicrobial agents tested by disk diffusion method have been included in Table S3 in the Supporting Information. The test results suggest that some of the pseudo-gemini surfactants are more effective against *Bacillus anthracis* than certain standard antibacterial drugs. However, further detailed study is needed to verify the effect of surfactants on this microorganism.

In one of the previous studies inhibitory effect of the pseudo-gemini amphiphiles based on ethyl piperazine and fatty acids on the same test organisms was investigated [43]. Overall average antimicrobial performance of the piperazine-based surfactants is relatively better than that of analogous ethyl piperazine-based surfactants. Analysis of the results from both studies indicates that molecular structures of both hydrophobic and hydrophilic groups of pseudo-gemini type amphiphiles are determining factors for antimicrobial performance. Piperazine based surfactants have two OH groups in the hydrophilic structure against the single OH group of the ethyl piperazine based analogues. In addition, highest antimicrobial performance in both series of surfactants was observed when an unsaturated bond was present in the hydrophobic groups. Therefore, it is possible to conclude that introducing various functional groups and unsaturated bonds into the molecular structure can positively affect the antimicrobial performance of pseudo-gemini type surfactants.

4.5. DPD simulation

4.5.1. Micelle morphology

The effect of surfactant concentration on morphology of micelles can be observed from Fig. 4. Red beads represent CO beads, blue beads represent NH beads, purple beads represent iOH beads. C beads are represented by light grey, whereas C1 = and C2 = beads are represented by dark grey. Water beads are hidden from the snapshots for clarity. The size of the clusters formed by carboxylic acid beads is increasing with increasing concentration. All CO beads are aligned away from the core of the clusters, which is in-line with the notion of normal geometric structure of surfactant micelles. A certain fraction of the counterion mesomolecules are interacting with the micellar clusters, while the remaining counterions are freely distributed in the solution. These findings indicate qualitative agreement between the real model of micellization process and the simulation.

4.5.2. Radial Distribution Function (RDF)

RDF describes the variation of particle density as a function of radial distance from the reference particle in a system comprised of multiple particles. RDF is the ratio of probability of finding another particle at a specific distance from the reference particle in a certain configuration of the system to the probability of finding a particle at the same distance from the same reference particle in a system of uniform particle distribution [44]. It provides a valuable insight into the structural arrangement of particles in various fluid systems including surfactant solutions. The RDF is calculated using the Eq. below [45]:

$$g(r) = \frac{\{dN_r(r \rightarrow r + dr)\}}{4\pi r^2 \rho dr} \quad (22)$$

where $dN_r(r \rightarrow r + dr)$ is the ensemble averaged number of particles at r distance from the reference particle, ρ is the number density of particles within the periodic cell.

The RDF of carboxylate groups of pseudo-gemini surfactants have been presented in Fig. 5. The data has been normalized to establish a comparison among different carboxylic acid chains at varying concentrations. The peaks on RDF curve imply orderly arrangement of the particles at short range. When a peak is high and sharp at a certain r distance, the connection between particles is strong and tight over that range. Each one of the RDF curves shown in Fig. 5 display a characteristic high peak seated at 5–6 Å. This corresponds to the average bond length between neighboring beads of the carboxylate mesomolecules. The intensity of the first peak is greatest for C_{10}-$PiPO_2$-C_{10}, followed by $C_{18:3}$-$PiPO_2$-$C_{18:3}$, $C_{18:1}$-$PiPO_2$-$C_{18:1}$, C_{14}-$PiPO_2$-C_{14} and C_{18}-$PiPO_2$-C_{18}. A higher first peak in RDF plot of a micellar system expresses lower tendency towards micellization. RDF plots of the carboxylate groups show a second smaller and flatter peak, implying the presence of another orderly arrangement of particles beyond intramolecular range. The height of the second peak becomes greater at higher concentrations. Increased height of the second peak indicates the formation of aggregates. The intensity of the first peak relative to the second peak decreases with increasing concentration. At higher concentrations more aggregates are formed, therefore the probability of finding two particles which are part of a mutual aggregate increases, while the probability of finding two particles that are separated only by a bond's distance becomes smaller. The RDF curves show that the local density of carboxylate groups decreases continuously and approaches zero beyond the second peak. This indicates that the arrangement of carboxylate mesomolecules within the solution is not uniform and intermicellar distances have very low local concentration of the subject particles.

Table 4
Antimicrobial properties of gemini-like surfactants based on 1,4-di-(propane-2-olyl)-piperazine and fatty acids.

	C_{10}-$PiPO_2$-C_{10}	C_{12}-$PiPO_2$-C_{12}	C_{14}-$PiPO_2$-C_{14}	C_{16}-$PiPO_2$-C_{16}	C_{18}-$PiPO_2$-C_{18}	$C_{18:1}$-$PiPO_2$-$C_{18:1}$	$C_{18:3}$-$PiPO_2$-$C_{18:3}$
Microorganisms	Diameter of inhibition zone (mm)						
Escherichia coli	7	–	9	–	7	–	–
Pseudomonas aeruginosa	8	–	–	–	–	–	11
Klebsiella pneumoniae	7	–	7	–	–	15	–
Staphylococcus aureus	7	7	8	–	–	9	8
Bacillus anthracis	7	8	–	–	–	10	15
Candida albicans	15	–	–	9	8	9	9

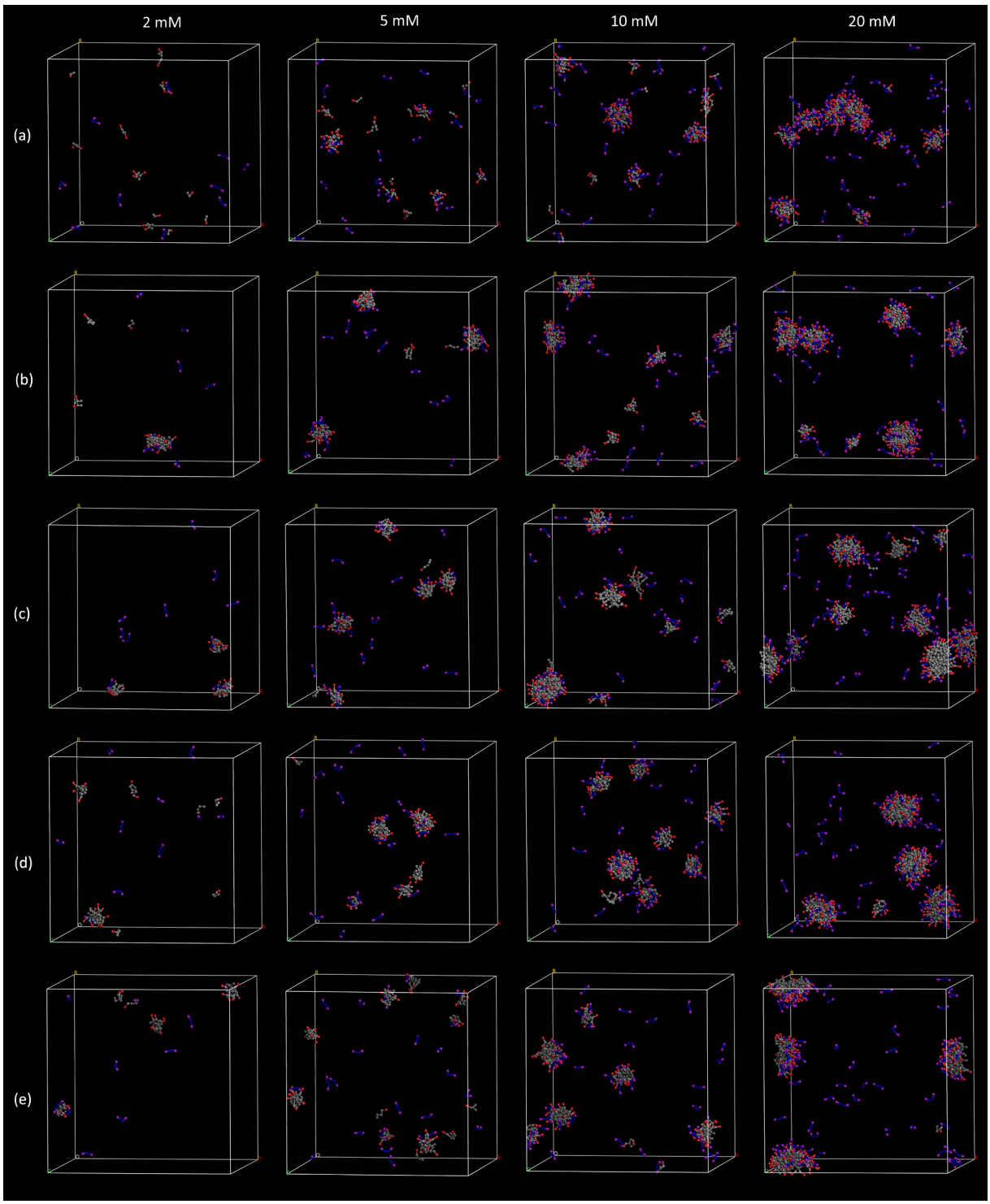

Fig. 4. Snapshots of equilibrated surfactant-water systems at different concentrations for (a) C_{10}-$PiPO_2$-C_{10}, (b) C_{14}-$PiPO_2$-C_{14}, (c) C_{18}-$PiPO_2$-C_{18}, (d) $C_{18:1}$-$PiPO_2$-$C_{18:1}$, (e) $C_{18:3}$-$PiPO_2$-$C_{18:3}$.

4.5.3. CMC prediction

The information extracted from DPD simulation trajectories can be utilized to theoretically evaluate CMC of the simulated surface-active compounds. A common method of theoretical CMC prediction is based on determining what fraction of the total dissolved surfactant molecules belong to micelles or are free from micelles. Two surfactant molecules are considered to belong to the same aggregate if their centers of mass are within a certain r_{agg} distance from each other. Moreover, to be considered as a micelle an aggregate should contain more than certain n_{mic} number of surfactant molecules. If the cluster contains less than n_{mic} number of surfactant molecules, all its contents are considered to be free from micelles. The concentration of the free surfactant molecules is counted as CMC [31,46,47].

The value of r_{agg} is determined from the RDF curve of the respective surfactant by locating the first neighbor minimum on the curve (see Fig. 5). The values of n_{mic} for each one of the pseudo-gemini surfactants were determined from the aggregate size distribution curves as the minimum point located between two peaks (see Fig. 6). n_{mic} varied by

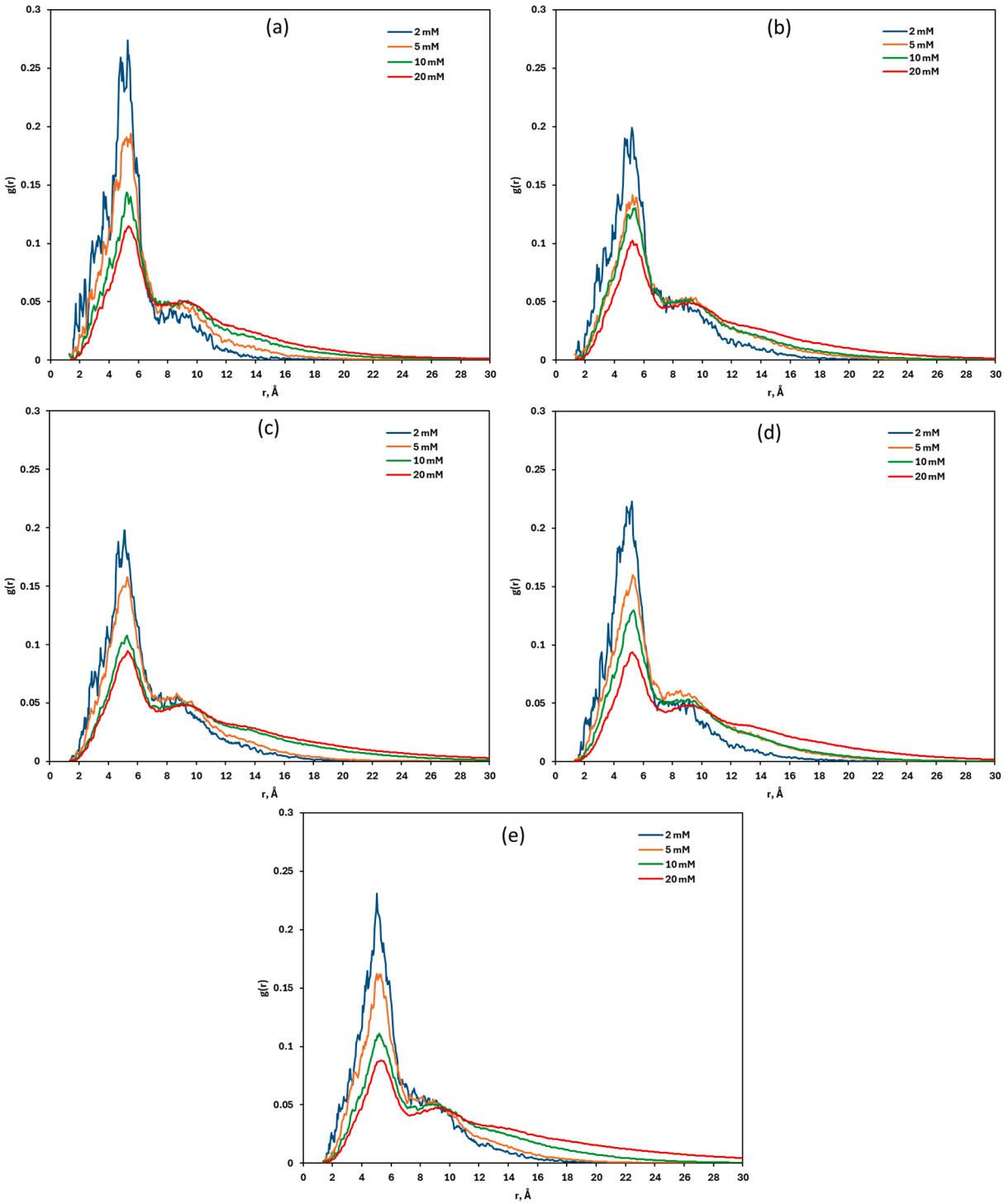

Fig. 5. Normalized RDF of carboxylate groups of pseudo-gemini surfactants at different concentrations for (a) C_{10}-$PiPO_2$-C_{10}, (b) C_{14}-$PiPO_2$-C_{14}, (c) C_{18}-$PiPO_2$-C_{18}, (d) $C_{18:1}$-$PiPO_2$-$C_{18:1}$, (e) $C_{18:3}$-$PiPO_2$-$C_{18:3}$.

concentration and carboxylate chain length and generally was between $n_{mic} = 5$ and $n_{mic} = 15$. The concentration of free surfactant molecules, aka CMC, was calculated for each one of the simulated pseudo-gemini surfactants at 2 mmol/L, 5 mmol/L, 10 mmol/L and 20 mmol/L system concentrations. Theoretically evaluated CMC values showed some fluctuation with changing bulk system concentration. However, no tendency to increase or decrease with increasing concentration was observed, and fluctuations were in acceptable range (see Fig. S10). The final calculated average CMC values were 1.887 mmol/L (C_{10}-$PiPO_2$-C_{10}) 1.086 mmol/L (C_{14}-$PiPO_2$-C_{14}), 0.910 mmol/L (C_{18}-$PiPO_2$-C_{18}), 1.046 mmol/L ($C_{18:1}$-$PiPO_2$-$C_{18:1}$), and 0.902 mmol/L ($C_{18:3}$-$PiPO_2$-$C_{18:3}$). Theoretical CMC values are higher than corresponding experimental CMC values listed in Table 3. However, trends in the variation of both experimental and theoretical CMC values with varying hydrophobic chain length and structure agree with each other (see Fig. S11).

4.5.4. *Radius of gyration evolution*

Radius of gyration (R_g) in general is the distance from the center of mass of a body at which the whole mass could be concentrated without changing its moment of rotational inertia about an axis through the

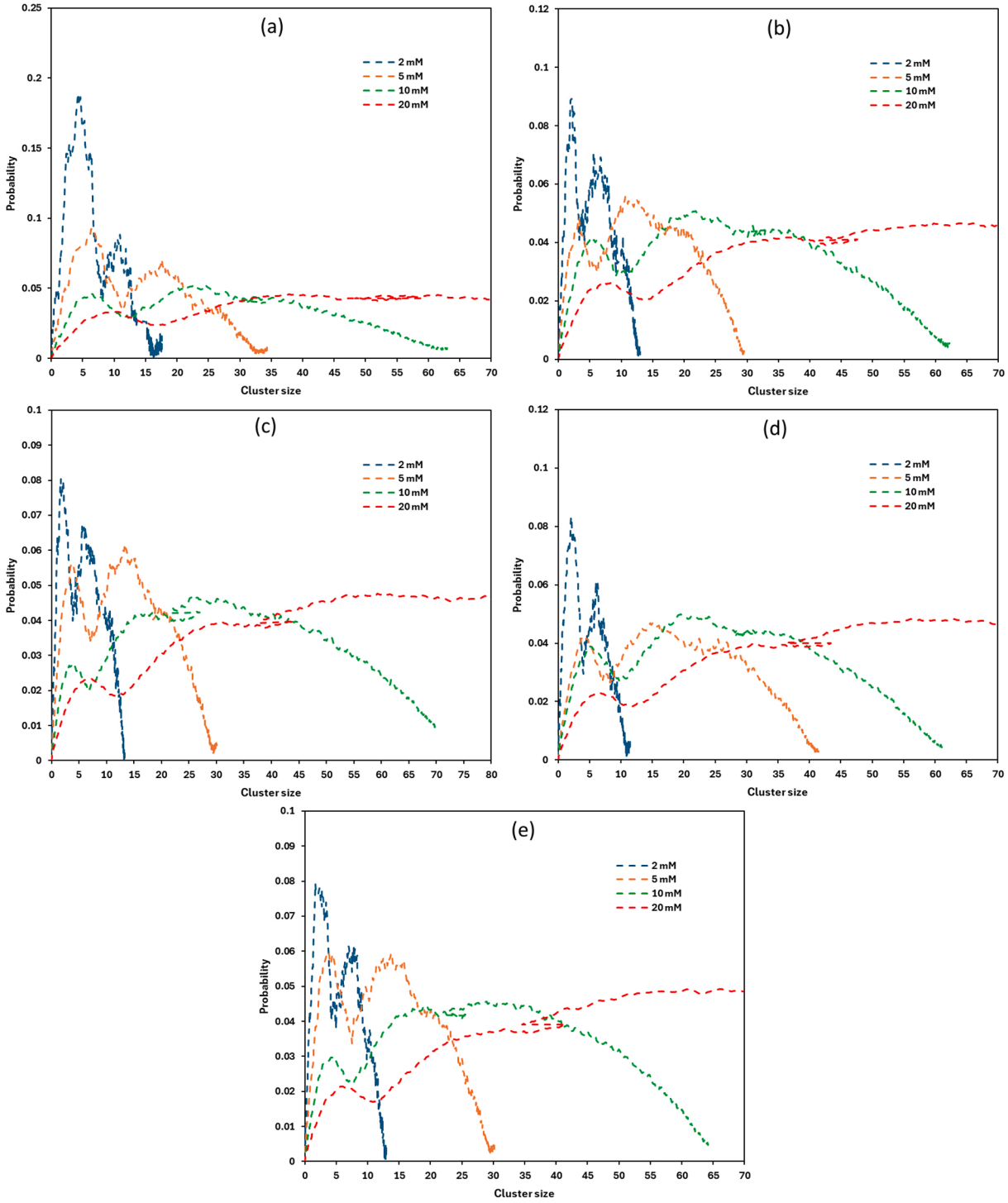

Fig. 6. Cluster size distribution curves for (a) C_{10}-$PiPO_2$-C_{10}, (b) C_{14}-$PiPO_2$-C_{14}, (c) C_{18}-$PiPO_2$-C_{18}, (d) $C_{18:1}$-$PiPO_2$-$C_{18:1}$, (e) $C_{18:3}$-$PiPO_2$-$C_{18:3}$ at different concentrations.

center of mass [48]. It provides valuable information related to orientation and structure of big molecules such as polymers and surfactants in solution environment. For a molecule consisting of different building blocks the radius of gyration is defined as the square root of the average squared distance of all the constituent units of the molecule from its center of mass and is expressed with the Eq. (23) below [48]:

$$R_g = \sqrt{\frac{1}{N}\sum_{i=1}^{N}\left(\vec{R}_i - \vec{R}_{CM}\right)^2} \quad (23)$$

where N is the total number of building blocks of the molecule, R_{CM} is the position of center of mass of the individual building blocks and R_i is the distance between centers of mass of the molecule and its constituent building blocks.

Determination of R_g of surfactant molecules helps to evaluate the level of curliness of the molecules. Higher values of R_g indicate that the molecules are 'stretched out' while lower values are observed for coiled conformations. Radius of gyrations of the pseudo-gemini surfactant molecules have been recorded throughout the simulation duration and

the results are presented in Fig. 7. At 2 mM concentration of saturated chain surfactants R_g increases first and then starts fluctuating around a certain value trying to reach equilibrium. At higher concentrations radius of gyration quickly attains its equilibrium value and exhibits very little fluctuation. Increased value of R_g indicates the transformation of molecules from coiled conformations to extended conformations. Structured arrangement of surfactant molecules within micelles restricts their coiling and results in increased value of R_g. Stabilization of R_g indicates the system has reached thermodynamic equilibrium. As Fig. 7 suggests, equilibrium configuration is reached more quickly when surfactant concentration is high. In addition, the equilibrium value of R_g is proportional to the total number of beads in the mesomolecule. However, despite having the same number of beads in their carboxylate mesomolecules, C_{18}-$PiPO_2$-C_{18}, $C_{18:1}$-$PiPO_2$-$C_{18:1}$, and $C_{18:3}$-$PiPO_2$-$C_{18:3}$ have differing equilibrium values of R_g. At a given concentration R_g of C_{18}-$PiPO_2$-C_{18} is greatest, followed by that of $C_{18:1}$-$PiPO_2$-$C_{18:1}$, and $C_{18:3}$-$PiPO_2$-$C_{18:3}$, indicating higher degree of coiling of the latter two. This result is in-line with the bent geometry of carboxylate groups of $C_{18:1}$-$PiPO_2$-$C_{18:1}$ and $C_{18:3}$-$PiPO_2$-$C_{18:3}$. Overall, R_g of carboxylate groups of $C_{18:1}$-$PiPO_2$-$C_{18:1}$ and $C_{18:3}$-$PiPO_2$-$C_{18:3}$ show more

Fig. 7. Radius of gyration evolution of carboxylate groups of pseudo-gemini surfactants at different concentrations for (a) C_{10}-$PiPO_2$-C_{10}, (b) C_{14}-$PiPO_2$-C_{14}, (c) C_{18}-$PiPO_2$-C_{18}, (d) $C_{18:1}$-$PiPO_2$-$C_{18:1}$, (e) $C_{18:3}$-$PiPO_2$-$C_{18:3}$.

fluctuations due to equilibrium values of bond angles [C]–[C1=]–[C], [C1=]–[C2=]–[C1=], [C]–[C1=]–[C2=] and [C1=]–[C]–[C] being smaller than 180°.

5. Conclusions

A series of pseudo-gemini type surfactants with identical hydrophilic groups, identical spacers and different hydrophobic have been prepared using piperazine, propylene oxide and carboxylic acids. The surfactants exhibited high surface activity with surface tension reduction being highest for short chain pseudo-gemini amphiphiles. Critical micelle concentration (CMC) of each one of the pseudo-gemini surfactants was lower than 1 mmol/L and varied little with alkyl chain length of the hydrophobic groups. Relatively lower solubility of pseudo-gemini surfactants with long saturated alkyl chains caused their CMC values to be higher than anticipated. Overall, the negative impact of lower solubility of saturated long alkyl groups and bent geometry of unsaturated alkyl groups on adsorption and micellization properties was observed. DLS measurements revealed the formation of large complex micellar aggregates in solutions of pseudo-gemini surfactants C_{16}-PiPO_2-C_{16}, C_{18}-PiPO_2-C_{18} and $C_{18:1}$-PiPO_2-$C_{18:1}$. Antimicrobial activity of C_{10}-PiPO_2-C_{10}, $C_{18:1}$-PiPO_2-$C_{18:1}$ and $C_{18:3}$-PiPO_2-$C_{18:3}$ was higher compared to other surface-active compounds. Dissipative Particle Dynamics (DPD) simulations could effectively predict micellization behavior of the pseudo-gemini surfactants. The effect of concentration, hydrophobic chain length and structure on aggregation behavior of the surfactants was observed on the normalized RDF plots. Relative heights of the first and second RDF peaks indicate the tendency for aggregation increases in C_{10}-PiPO_2-C_{10} < $C_{18:3}$-PiPO_2-$C_{18:3}$ < $C_{18:1}$-PiPO_2-$C_{18:1}$ < C_{14}-PiPO_2-C_{14} < C_{18}-PiPO_2-C_{18} order. Theoretically predicted CMC values were in the same order of magnitude as the experimental CMC values, but slightly higher. Both experimental and theoretical CMCs followed a similar trend with varying hydrocarbon chain length. Radius of gyration plots of carboxylate mesomolecules indicated that the system reached equilibrated configuration of aggregates. The radius of gyration calculated for carboxylate groups $C_{18:1}$-PiPO_2-$C_{18:1}$ and $C_{18:3}$-PiPO_2-$C_{18:3}$ was smaller than that of C_{18}-PiPO_2-C_{18} which agrees with the bent geometry of oleate and linoleate ions. This was the outcome of selection of bond angles smaller than 180° for $C_{18:1}$-PiPO_2-$C_{18:1}$ and $C_{18:3}$-PiPO_2-$C_{18:3}$.

CRediT authorship contribution statement

Elgun E. Hasanov: Writing – review & editing, Writing – original draft, Software, Resources, Methodology, Investigation, Funding acquisition. **Ravan A. Rahimov:** Writing – original draft, Visualization, Supervision, Project administration. **Gulnara A. Ahmadova:** Formal analysis, Data curation. **Sevda A. Muradova:** Formal analysis, Data curation. **Atash V. Gurbanov:** Formal analysis, Data curation.

Declaration of competing interest

The authors declare that they have no known competing financial interests or personal relationships that could have appeared to influence the work reported in this paper.

Data availability

The authors do not have permission to share data.

Acknowledgements

This work was supported by the Fundação para a Ciência e a Tecnologia (FCT) (Portugal), projects UIDB/00100/2020 (DOI: 10.54499/UIDB/00100/2020), UIDP/00100/2020 (DOI: 10.54499/UIDP/00100/2020) of Centro de Química Estrutural and LA/P/0056/2020 (DOI: 10.54499/LA/P/0056/2020) of Institute of Molecular Sciences. A.V.G. is grateful to FCT and Instituto Superior Técnico (DL 57/2016 and L57/2017 Programs, Contract no: IST-ID/110/2018), as well as Baku Engineering University (Azerbaijan), Institute of Petrochemical Processes of the Ministry of Science and Education (Azerbaijan), Baku State University (Azerbaijan) and Western Caspian University (Azerbaijan).

Appendix A. Supplementary material

Supplementary data to this article can be found online at https://doi.org/10.1016/j.molliq.2024.125766.

References

[1] M.J. Rosen, D.J. Tracy, Gemini surfactants, J. Surfactants Deterg. 1 (1998) 547–554, https://doi.org/10.1007/s11743-998-0057-8.
[2] R. Sharma, A. Kamal, M. Abdinejad, R.K. Mahajan, H.B. Kraatz, Advances in the synthesis, molecular architectures and potential applications of Gemini surfactants, Adv. Colloid Interface Sci. 248 (2017) 35–68, https://doi.org/10.1016/j.cis.2017.07.032.
[3] L. Guerrero-Hernández, H.I. Meléndez-Ortiz, G.Y. Cortez-Mazatan, S. Vaillant-Sánchez, R.D. Peralta-Rodríguez, Gemini and bicephalous surfactants: a review on their synthesis, micelle formation, and uses, Int. J. Mol. Sci. 23 (2022) 1798, https://doi.org/10.3390/ijms23031798.
[4] B.E. Brycki, I.H. Kowalczyk, A. Szulc, O. Kaczerewska, M. Pakiet, Multifunctional gemini surfactants: structure, synthesis, properties and applications, p. Ch. 4, in: I. H. Kowalczyk (Ed.), Appl. Charact. Surfactants, IntechOpen, Rijeka, 2017, https://doi.org/10.5772/intechopen.68755.
[5] A. Bhattarai, M. Abdul Rub, M. Posa, B. Saha, D. Kumar, Catalytic impacts of cationic twin headed and tailed gemini surfactants toward study of glycine and ninhydrin in sodium acetate-acetic acid buffer system, J. Mol. Liq. 360 (2022) 119442, https://doi.org/10.1016/j.molliq.2022.119442.
[6] M. Posa, A. Bhattarai, J.M. Khan, B. Saha, D. Kumar, Impact of double headed geminis on leucine and ninhydrin reaction in buffer solvent, Colloids Surf. A Physicochem. Eng. Asp. 674 (2023) 131951, https://doi.org/10.1016/j.colsurfa.2023.131951.
[7] Y.G. Alghamdi, M.A. Rub, D. Kumar, Influence of twin-headed gemini micellar system on the study of methionine amino acid with ninhydrin in buffer solution, R. Soc. Open Sci. 10 (2023) 221249, https://doi.org/10.1098/rsos.221249.
[8] D. Kumar, J.M. Khan, M. Posa, A.K. Pulikkal, B. Saha, A. Bhattarai, Effect of quaternary ammonium Gemini surfactant solution on the rate constant of the Ninhydrin-lysine reaction, Ind. Eng. Chem. Res. 62 (2023) 15897–15906, https://doi.org/10.1021/acs.iecr.3c02499.
[9] N. Kampf, C. Wu, Y. Wang, J. Klein, A trimeric surfactant: surface micelles, hydration-lubrication, and formation of a stable, charged hydrophobic monolayer, Langmuir. 32 (2016) 11754–11762, https://doi.org/10.1021/acs.langmuir.6b02657.
[10] T. Morita, S. Yada, T. Yoshimura, Linear- and star-type quaternary ammonium salt-based trimeric surfactants: effect of structure on adsorption and aggregation properties, Colloids Surf. A Physicochem. Eng. Asp. 656 (2023) 130364, https://doi.org/10.1016/j.colsurfa.2022.130364.
[11] W.A. El-Said, A.S. Moharram, E.M. Hussein, A.M. El-Khawaga, Synthesis, characterization, and applications of some new trimeric-type cationic surfactants, J. Surfact. Deterg. 21 (2018) 343–353, https://doi.org/10.1002/jsde.12041.
[12] Y. Xie, J. Li, Z. Li, T. Sun, Y. Wang, G. Qu, The adsorption and aggregation properties of dendritic cationic tetrameric surfactants, RSC Adv. 8 (2018) 36015–36024, https://doi.org/10.1039/c8ra06900j.
[13] Y. Hou, Y. Han, M. Deng, J. Xiang, Y. Wang, Aggregation behavior of a tetrameric cationic surfactant in aqueous solution, Langmuir. 26 (2010) 28–33, https://doi.org/10.1021/la903672r.
[14] H. Wu, B. Fang, L. Yu, J. He, W. Xu, H. Xin, Z. Tian, X. Han, Y. Lu, K. Xu, Rheology and delayed micellar formation process of novel tetrameric cationic surfactant fracturing fluid, J. Surfactants Deterg. 26 (2023) 827–842, https://doi.org/10.1002/jsde.12693.
[15] R. Zana, J. Xia, Gemini Surfactants: Synthesis, Interfacial and Solution-Phase Behavior, and Applications, CRC Press, 2003.
[16] H. Jia, X. Leng, P. Lian, Y. Han, Q. Wang, S. Wang, T. Sun, Y. Liang, P. Huang, K. Lv, pH-Switchable IFT variations and emulsions based on the dynamic noncovalent surfactant/salt assembly at the water/oil interface, Soft Matter. 15 (2019) 5529–5536, https://doi.org/10.1039/c9sm00891h.
[17] Y. Zhang, J. Qi, N. Wang, L. Wang, H. Lu, Pseudo gemini surfactant fracturing fluid with dual function of fracturing and oil flooding for enhanced oil recovery, J. Mol. Liq. 393 (2023) 123562, https://doi.org/10.1016/j.molliq.2023.123562.
[18] S. Ye, Z. Zhai, S. Shang, Z. Song, pH-Induced hydrogels and viscoelastic solutions constructed by a Rosin-Based Pseudo-Gemini surfactant, J. Mol. Liq. 361 (2022) 119445, https://doi.org/10.1016/j.molliq.2022.119445.
[19] X. Wei, X. He, D. Zhang, X. Su, CO2-responsive wormlike micelles based on pseudo-tetrameric surfactant, Molecules. 27 (2022) 7922, https://doi.org/10.3390/molecules27227922.
[20] Z. Chen, D. Xie, B. Song, C. Li, X. Pei, R. Li, Worm-like micelles constructed by "pseudo" tetrameric surfactants containing azobenzene groups, J. Mol. Liq. 316 (2020) 113847, https://doi.org/10.1016/j.molliq.2020.113847.

[21] F.O. Nitbani, P.J.P. Tjitda, B.A. Nurohmah, H.E. Wogo, Preparation of fatty acid and monoglyceride from vegetable oil, J. Oleo Sci. 69 (2020) 277–295, https://doi.org/10.5650/jos.ess19168.
[22] S. Sharma, N. Anand, Chapter 5 Piperazines, in: S. Sharma, N.-B.-T.-.-P.-L. Anand (Eds.), Pharmacochem. Libr., Elsevier, 1997, pp. 148–170, https://doi.org/10.1016/S0165-7208(97)80027-X.
[23] T.A. Nijhuis, M. Makkee, J.A. Moulijn, B.M. Weckhuysen, The production of propene oxide: catalytic processes and recent developments, Ind. Eng. Chem. Res. 45 (2006) 3447–3459, https://doi.org/10.1021/ie0513090.
[24] P.K. Sundaram, M.M. Sharma, Kinetics of reactions of amines with alkene oxides, Bull. Chem. Soc. Jpn. 42 (1969) 3141–3147, https://doi.org/10.1246/bcsj.42.3141.
[25] J.Ž. Manojlović, The Krafft temperature of surfactant solutions, Therm. Sci. 16 (2013) 631–640, https://doi.org/10.2298/TSCI120427197M.
[26] P.J. Hoogerbrugge, J.M.V.A. Koelman, Simulating microscopic hydrodynamic phenomena with dissipative particle dynamics, Europhys. Lett. 19 (1992) 155, https://doi.org/10.1209/0295-5075/19/3/001.
[27] P. Español, P. Warren, Statistical mechanics of dissipative particle dynamics, Europhys. Lett. 30 (1995) 191, https://doi.org/10.1209/0295-5075/30/4/001.
[28] R.D. Groot, K.L. Rabone, Mesoscopic simulation of cell membrane damage, morphology change and rupture by nonionic surfactants, Biophys. J. 81 (2001) 725–736, https://doi.org/10.1016/S0006-3495(01)75737-2.
[29] R.D. Groot, P.B. Warren, Dissipative particle dynamics: bridging the gap between atomistic and mesoscopic simulation, J. Chem. Phys. 107 (1997) 4423–4435, https://doi.org/10.1063/1.474784.
[30] R.L. Anderson, D.J. Bray, A.S. Ferrante, M.G. Noro, I.P. Stott, P.B. Warren, Dissipative particle dynamics: systematic parametrization using water-octanol partition coefficients, J. Chem. Phys. 147 (2017), https://doi.org/10.1063/1.4992111.
[31] Z. Mai, E. Couallier, M. Rakib, B. Rousseau, Parameterization of a mesoscopic model for the self-assembly of linear sodium alkyl sulfates, J. Chem. Phys. 140 (2014) 204902, https://doi.org/10.1063/1.4875515.
[32] M.B. Liu, G.R. Liu, L.W. Zhou, J.Z. Chang, Dissipative Particle Dynamics (DPD): an overview and recent developments, Arch. Comput. Methods Eng. 22 (2015) 529–556, https://doi.org/10.1007/s11831-014-9124-x.
[33] Y. Li, H. Zhang, M. Bao, Q. Chen, Aggregation behavior of surfactants with different molecular structures in aqueous solution: DPD simulation study, J. Dispers. Sci. Technol. 33 (2012) 1437–1443, https://doi.org/10.1080/01932691.2011.620897.
[34] R.L. Anderson, D.J. Bray, A. Del Regno, M.A. Seaton, A.S. Ferrante, P.B. Warren, Micelle formation in alkyl sulfate surfactants using dissipative particle dynamics, J. Chem. Theory Comput. 14 (2018) 2633–2643, https://doi.org/10.1021/acs.jctc.8b00075.
[35] F. Goodarzi, S. Zendehboudi, Effects of salt and surfactant on interfacial characteristics of water/oil systems: Molecular dynamic simulations and dissipative particle dynamics, Ind. Eng. Chem. Res. 58 (2020) 8817–8834, https://doi.org/10.1021/acs.iecr.9b00504.
[36] E. Lavagnini, J.L. Cook, P.B. Warren, M.J. Williamson, C.A. Hunter, A surface site interaction point method for dissipative particle dynamics parametrization: application to alkyl ethoxylate surfactant self-assembly, J. Phys. Chem. B. 124 (2020) 5047–5055, https://doi.org/10.1021/acs.jpcb.0c01895.
[37] M.J. Rosen, J.T. Kunjappu, Surfactants and Interfacial Phenomena, fourth ed., Wiley, 2012, 10.1002/9781118228920.
[38] Z.X. Li, C.C. Dong, R.K. Thomas, Neutron reflectivity studies of the surface excess of gemini surfactants at the air-water interface, Langmuir. 15 (1999) 4392–4396, https://doi.org/10.1021/la981551u.
[39] B.L. Bales, A definition of the degree of ionization of a micelle based on its aggregation number, J. Phys. Chem. b. 105 (2001) 6798–6804, https://doi.org/10.1021/jp004576m.
[40] G. Sugihara, M. Hisatomi, Roles of counterion binding in the micelle formation of ionic surfactants in water, J. Jpn. Oil Chem. Soc. 47 (1998) 1–24.
[41] R. Zana, Critical micellization concentration of surfactants in aqueous solution and free energy of micellization, Langmuir. 12 (1996) 1208–1211, https://doi.org/10.1021/la950691q.
[42] M. Qi, Y. Zhou, Multimicelle aggregate mechanism for spherical multimolecular micelles: from theories, characteristics and properties to applications, Mater. Chem. Front. 3 (2019) 1994–2009, https://doi.org/10.1039/c9qm00442d.
[43] E.E. Hasanov, R.A. Rahimov, Y. Abdullayev, G.A. Ahmadova, Symmetric and dissymmetric pseudo-gemini amphiphiles based on propoxylated ethyl piperazine and fatty acids, ChemistrySelect. 8 (2023) e202303942.
[44] T. Fan, L. Chen, X. Xia, Y. Wu, J. Zhang, K. Yin, F. Liu, Z. Yan, Dissipative particle dynamics quantitative simulation of the formation mechanism and emulsification driving force of deep eutectic solvent-based surfactant-free and water-free microemulsion, Ind. Eng. Chem. Res. 60 (2021) 3249–3258, https://doi.org/10.1021/acs.iecr.0c06193.
[45] J.P. Hansen, I.R. McDonald, Theory of Simple Liquids, third ed., Elsevier Science, 2006, 10.1016/B978-0-12-370535-8.X5000-9.
[46] S.J. Marrink, D.P. Tieleman, A.E. Mark, Molecular dynamics simulation of the kinetics of spontaneous micelle formation, J. Phys. Chem. b. 104 (2000) 12165–12173, https://doi.org/10.1021/jp001898h.
[47] A. Vishnyakov, M.T. Lee, A.V. Neimark, Prediction of the critical micelle concentration of nonionic surfactants by dissipative particle dynamics simulations, J. Phys. Chem. Lett. 4 (2013) 797–802, https://doi.org/10.1021/jz400066k.
[48] A. Rudi, P. Cho, The Elements of Polymer Science and Engineering, Academic Press (2012), https://doi.org/10.1016/C2009-1-64286-6.